A R C H I V E S O F M E T A L L U R G Y A N D M A T E R I A L S
Volume 60 2015 Issue 2
DOI: 10.1515/amm-2015-0228

M. JANUŚ*,♯, K. KYZIOŁ*, S. KLUSKA*, J. KONEFAŁ-GÓRAL*, A. MAŁEK*, S. JONAS*

PLASMA ASSISTED CHEMICAL VAPOUR DEPOSITION – TECHNOLOGICAL DESIGN OF FUNCTIONAL COATINGS

CHEMICZNE OSADZANIE Z FAZY GAZOWEJ WSPOMAGANE PLAZMOWO – PROJEKTOWANIE TECHNOLOGII FUNKCJONALNYCH POWŁOK

Plasma Assisted Chemical Vapour Deposition (PA CVD) method allows to deposit of homogeneous, well-adhesive coatings at lower temperature on different substrates. Plasmochemical treatment significantly impacts on physicochemical parameters of modified surfaces. In this study we present the overview of the possibilities of plasma processes for the deposition of diamond-like carbon coatings doped Si and/or N atoms on the Ti Grade2, aluminum-zinc alloy and polyetherketone substrate. Depending on the type of modified substrate had improved the corrosion properties including biocompatibility of titanium surface, increase of surface hardness with deposition of good adhesion and fine-grained coatings (in the case of Al-Zn alloy) and improving of the wear resistance (in the case of PEEK substrate).

Keywords: PA CVD, titanium, aluminum alloys, polyetheretherketone, ceramic coatings

Metoda chemicznego otrzymywania warstw z fazy gazowej w warunkach plazmy (PA CVD – *Plasma Assisted Chemical Vapour Deposition)* umożliwia otrzymywanie homogenicznych struktur warstwowych w niskich temperaturach, o dobrej adhezji do podłoży. Warunki w jakich prowadzone są procesy plazmochemiczne w znacznym stopniu decydują o właściwościach fizykochemicznych modyfikowanych powierzchni. W pracy przedstawiono możliwości w zakresie projektowania procesów plazmochemicznych z otrzymaniem warstw DLC (Diamond-like Carbon) dotowanych atomami Si i/lub N. W zależności od rodzaju modyfikowanego podłoża uzyskano poprawę właściwości korozyjnych przy zachowaniu biokompatybilności powierzchni (w przypadku Ti Grade2), poprawę twardości powierzchni na drodze otrzymania drobnoziarnistej powłoki o dobrej adhezji do podłoża (w przypadku Al-Zn) i poprawę odporności na zużycie (w przypadku PEEK).

1. Introduction

Chemical vapor deposition method assisted plasma is currently the most effective technique to obtain a variety of layers on ceramic substrates, metals, alloys, polymers, at relatively low temperatures, even at room temperature. These layers are very good adhesion to the substrate due to the existence of chemical bonds between the coating and the substrate. These surface modification techniques allow to obtain layers with very good performance for many materials. Improve the tribological properties and corrosion resistance of metals (Titanium) and alloys. In the case of titanium increase its biocompatibility and affect their cytotoxicity [1-3]. It is established that for successful application of polymeric composite materials to form structural parts using adhesive bonding, they need to have particular properties regarding topography (roughness) and/or surface chemistry (polar functionalities) [4]. Modification of the polymer surface can be carried out by etching, cross-linking or plasma treatment [5-7]. These processes increase surface roughness and extend the contact area between the material and the environment that results in forming structures in the surface layer more strongly bounded to the substrate.

In this study we present the results of application of PA CVD method for the modification of the surface of Ti, Al-Zn Alloy and polyetheretherketone (PEEK).

2. Experimental

The surfaces modifications studied in this work were applied on unalloyed Ti (Grade2), Al-Zn alloy and polyetherketone (PEEK) using the MW-RF CVD system, shown in Fig. 1.

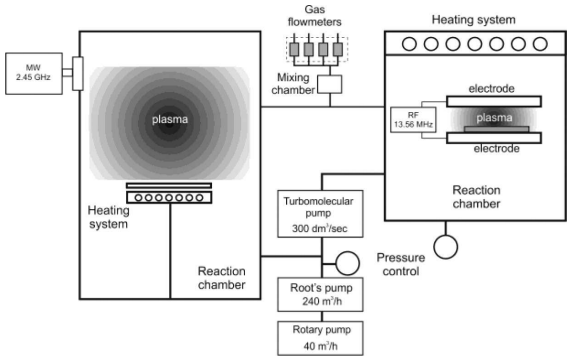

Fig. 1. Schematic diagram of MW-RF CVD equipment

* AGH UNIVERSITY OF SCIENCE AND TECHNOLOGY, AL. A. MICKIEWICZA 30, 30-059 KRAKÓW, POLAND
♯ Corresponding author: martaj@agh.edu.pl

TABLE 1

Details for plasma modification including carbon-based coatings deposition

Substrate	Type of plasmochemical proces	Technological parameters				
		Gas/flow [sccm]	$P_{RF/MW}$ [W]	T_s [°C]	p [Tr]	t [min]
Ti Grade2	SiCH	Ar/225; CH_4/25; SiH_4/3	P_{MW} 400	600	0.3	30
	SiNH	Ar/225; NH_3/150; SiH_4/3	P_{MW} 400	600	0.3	30
	SiCNH	Ar/225; NH_3/130; CH_4/20; SiH_4/3	P_{MW} 400	600	0.3	30
Al-Zn alloy	N^+ ion	N_2/90; H_2/30	P_{RF} 100	350	0.7	120
	Si-DLC	Ar/80; SiH_4/8; CH_4/8	P_{RF} 50	400	0.4	8
Polyetherketone	CNH	Ar/75; N_2/85; CH_4/10	P_{RF} 80	24	0.4	30
	SiCNH	Ar/75; N_2/25; CH_4/104; SiH_4/3	P_{RF} 80	24	0.4	30

Carbon-based coatings, including of SiCH, SiNH, SiCNH, CNH and N^+ ion modification process in plasma conditions were prepared onto selected substrates – see TABLE 1.

$P_{RF/MW}$ – radio-frequency or micro-wave generator power, T_s – substrate temperature, p – pressure in the reactor, t – time of process deposition.

Before substrate functionalization, ion modification and/or deposition of carbon-based layers of the surfaces of substrate were cleaned in argon plasma, which is effective for many types of contaminations such as metal oxides, organic compounds, *etc.*.

The measurements of the chemical composition and surface morphology for the obtained coatings were performed on a Scanning Electron Microscope and Energy Dispersive Spectrometer techniques. The structure in atomic-scale of the studied samples was revealed by IR spectroscopy. The FTIR spectra were measured within 400÷4000 cm^{-1} using Bio-Rad FTS 60V spectrometer.

Selected samples were investigated by XPS, AFM, XRD method, nanoindentation technique and corrosion and biological tests. The XPS measurements were performed with use of the monochromatized Al K_α X-ray source ($h\nu$ =1486.6 eV). All spectra were calibrated to binding energy value of the C 1s peak at 285.0 eV. The analysis was performed for "fresh" ex situ surface and after sputtering process by Ar^+ ions with the energy 2 keV. The characteristic of surface region was obtained from XPS depth profile. Surface topography was analyzed with an AFM – atomic force microscopy instrument. Phase composition of the samples was identified on the basis of X-ray diffraction analysis (XRD) performed with an HZG-4 apparatus with CuKα radiation.

The microhardness profiles (hardness and Young modulus) have been obtained by using nanoindentation technique. Frictional and wear research in rotating samples were performed on a dry ball-plane contact using a ball-disc tribotester, in according to the requirements specified in ASTM G 99-05, ISO 20808-2004 standards.

The contact angles were measured by the sessile drop method using the automatic drop shape analysis system.

The study of corrosion resistance were investigated using accelerated techniques for polarization in the three-electrode system (working electrode – the test sample, the reference electrode – chloride-silver electrode Ag/AgCl/Cl^-, electrode – platinum electrode) in synthetic biological solutions (Ringer solution and artificial saliva).

Preliminary biological tests have included studies on the cytotoxicity of the modified titanium and their biocompatibility.

3. Results and Discussion

3.1. Ceramics layers on titanium

Approximate composition of the obtaining layers on Ti substrate shows Fig. 2. The selected composition of $SiC_xN_y(H)$ layer has the best usable properties.

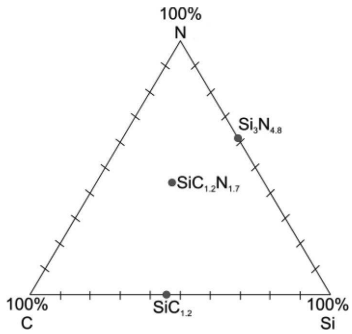

Fig. 2. C-Si-N Gibbs triangle with marked indicative warehouses resulting chemical compounds identified in the EDS measurements

The thickness of obtained under the above conditions the layers is varied and depends on their chemical composition (for $Si_xN_y(H)$ about 73 nm, for $SiC_x(H)$ – 115 nm, for $SiC_xN_y(H)$ – 195 nm). The layers are homogeneous and well adhere to the substrate.

The XRD studies have shown that a substrate with $SiC_xN_y(H)$ layer comprises titanium compounds both with carbon and nitrogen – Fig. 3. Other layers are amorphous because they do not provide the X-ray spectra.

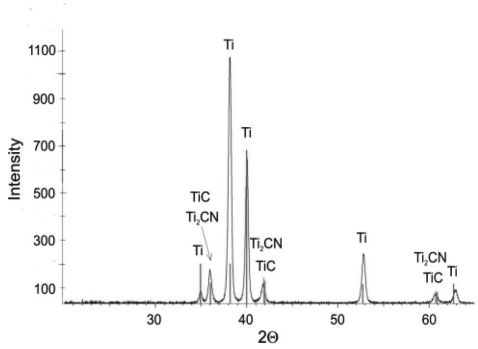

Fig. 3. X-ray analize of Ti samples with $SiC_xN_y(H)$ layer

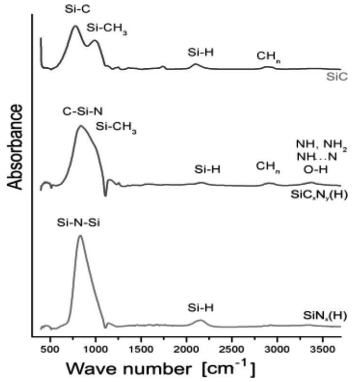

Fig. 4. FT IR spectra of (001)Si substrate

Fig. 4 shows transmission FT IR spectra of the layers deposited on the (001)Si substrate for the characterization of phase composition of layers. At the spectra of the silicon nitride layer ($SiN_x(H)$) is dominant band at about 835 cm^{-1} derived from the stretching vibration of Si-N-Si. In its structure are also bands of type Si-H (about 2165 cm^{-1}). In the spectra of silicon carbide ($SiC_x(H)$) shows the bands of the vibration of Si-C (about 780 cm^{-1}) and Si-CH_3 (about 990 cm^{-1}) and a low bands around 1250 cm^{-1}, 2105 cm^{-1}, and 2895 cm^{-1} (C-H_n). At the spectra of the silicon carbonitride layer ($SiC_xN_y(H)$) is a wide band of a complex structure in the range 600 cm^{-1} – 1100 cm^{-1}. This spectra is not a characteristic of Si-C and Si-N groups Therefore, it can be concluded that the complex chemical silicon carbide layer and silicon nitride does not appear as a separate phases. Silicon is here surrounded by both nitrogen and also carbon. Next to it at spectra are low bands in 1255 cm^{-1} and 1360 cm^{-1} caused by vibrations of the Si-$(CH_3)_x$, 2160 cm^{-1} (Si-H) and 2820 cm^{-1} (CH_n).

The next step was to examine the effect of such modified materials on their usable properties: friction coefficient, wear resistance and corrosion resistance. Moreover, it was performed preliminary biological tests such as cytotoxicity and biocompatibility.

Fig. 5 shows the results of measurements of the friction coefficient. The total measuring range, up to 500 cycles, the friction coefficient for the unmodified surface of Ti is the highest and reaches a maximum value of 0.46. All tested layers cause an improvement of sliding properties of titanium. The sample with $Si_xN_y(H)$ layer and $SiC_xN_y(H)$ layer have a very good sliding properties up to about 350 cycles (f <0.1), then the friction increases as a result of interruption of layers. However, even after the removal of them value of is maintained at a lower level than for the Ti substrate. The worst sliding properties has a $SiC_x(H)$ layer (threshold value of the cycle – about 100), due to the fragility of the silicon carbide.

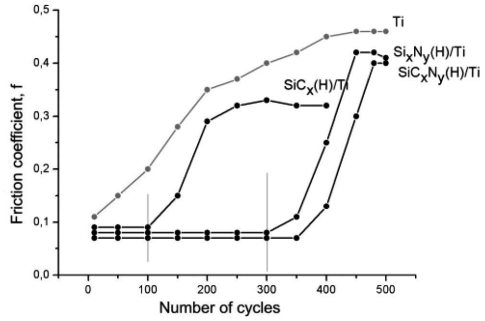

Fig. 5. Comparison of average friction coefficients determined for samples of raw titanium and after modification

The last one of tribological properties which was studied it was wear resistance of tests samples. All layers significantly improve the abrasion resistance of Ti, with the most efficient silicon carbonitride layer (W_v = 39.5±13.3 mm^3/Nm). The wear indicator is more than four times lower than the indicator for the starting material.

Corrosion resistance was assessed for the unmodified substrate and Ti with $SiC_xN_y(H)$ layer because of it has the best tribological properties. Comparing the corrosion potential (E_{cor}) of raw Ti substrate and the substrate with the $SiC_xN_y(H)$ during the exposition in Ringer solution (Fig. 6a) clearly shows the effect of the surface structure on E_{cor} value. In the case of the first material is about -0.18 V. The layer a value of E_{cor} is almost three times lower and amounts to about -0.4 V. For a more aggressive environment, which is the artificial saliva solution, the situation is somewhat different – Fig. 6b. Corrosion potential values for both materials are quite similar (raw Ti – 0.45 V, Ti with the layer of about -0.4 V).

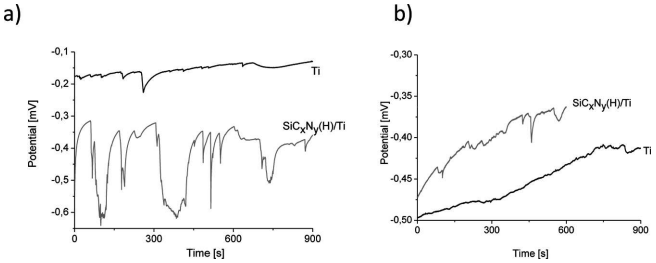

Fig. 6. Corrosion potentials of the raw Ti and after modification when exposed to Ringer's solution (a) and the artificial saliva (b) in temperature 37°C for 15 minutes

The current density dependence of the potential for both environments showed that the layer does not deteriorate the corrosion resistance of titanium – Fig. 7a,b. Practically curves for both tested materials did not stray far from each other. The $SiC_xN_y(H)$ layer shows a list of characteristics in the barrier coating. This layer, similar to the titanium oxide, has a wide range passive until the potential of 1.5 V.

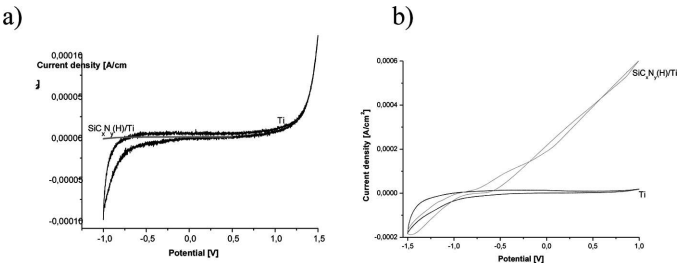

Fig. 7. The current density dependence of the potential of the raw Ti and after modification when exposed to Ringer's solution (a) and the artificial saliva (b) in temperature 37°C

The LSV (linear sweat voltametry) tests were confirmed in chrono-amperometric studies – Fig.8 a,b.

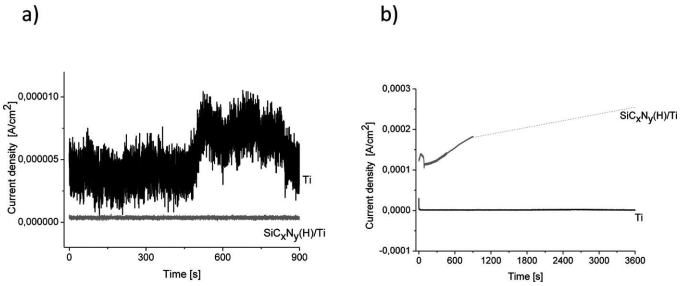

Fig. 8. Chrono-amperometric curves at E = E_{cor} + 100 mV of the raw Ti and after modification when exposed to Ringer's solution (a) and the artificial saliva (b) in temperature 37°C

The studies of corrosion resistance was supplemented by measurements of the chemical composition of both solutions. Applying a coating with silicon substantially reduces about six-times the passage of the substrate material to the corrosive environment. The amounts of material of surface for modified titanium are much lower in both solutions than raw Ti.

The SEM/EDS results obtained after the corrosion process, in order to compare the microstructure and chemical composition of raw samples and after modification. For samples with the SiC$_x$N$_y$(H) layer does not see any signs of degrading action of the two test solutions. Visually, without using a microscope, it can be concluded that the layer is not affected.

Preliminary biological tests consisted in demonstrating that the modification of titanium does not cause significant increase in its cytotoxicity and checking their biocompatibility.

An estimate of the fraction of viable colons cancer of mouse cells – CT26 (S) to the dead cells (S_0) after 72 hours of incubation. The ratio is slightly larger than the layer of raw substrate, which is associated with a slight increase in cytotoxicity (within the measurement error). The concentration of CT26 cells is shown at Fig. 9a.

Biocompatibility tests SiC$_x$N$_y$(H) layer on Titanium was performed using osteoblast cells MG63. Discussed layer, as shown at Fig. 9b, is a very good breeding ground for these cells. We can conclude that its biocompatibility is very well.

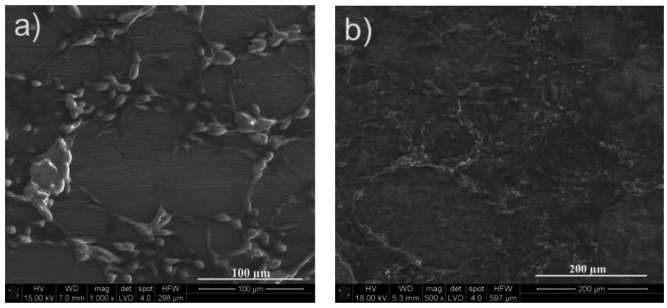

Fig. 9. SEM image of titanium with SiC$_x$N$_y$(H) layer after biological tests: (a) CT26 cells, (b) MG63 cells

3.2. Coatings on Al-Zn alloy

The Al-Zn alloy have been modified by three stages of plasmochemical process (plasma etching, N^+ ion modification and Si-DLC coating deposition, *vide supra* Table 1).

It has been observed that the microstructure of surfaces after modification was homogenous, fine granular structure of the coating (*ca.* 30 nm of grain size and *ca.* 1.5 nm of surface roughness) and without any defects – see Fig. 10.

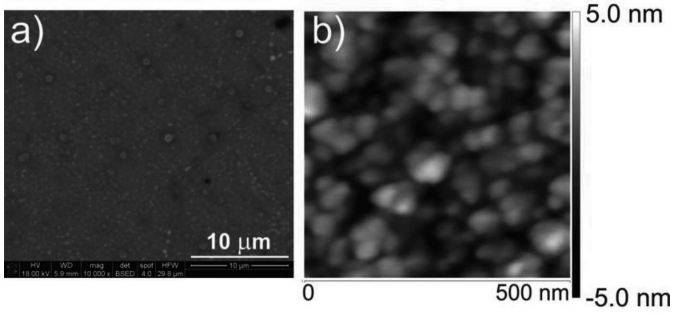

Fig. 10. SEM (a) and AFM (b) images of Al-Zn substrate after surface modification in plasma conditions (plasma etching, N^+ ion modification and Si-DLC deposition)

Moreover, the analysis of EDS spectra have revealed that plasma processes significantly determines the chemical content of the surface. The chemical composition of Al-Zu substrate after modification has shown the presence of Si, C and N atoms content in the comparison to the unmodified samples.

In details, the surface modification of Al-Zn substrate the following EDS analysis has been obtained: 10.13 % wt. C, 8.64 % wt. N, 1.12 % wt. O, 2.30 % wt. Mg, 65.09 % wt. Al, 14.88 % wt. Si, 0.77 % wt. Fe, 1.26 % wt. Cu, 3.80 % wt. Zn, for plasma etching, nitrogenation and Si-DLC deposition process; 3.16% wt. Mg, 90.66% wt. Al, 6.18% wt. Zn for unmodified aluminium alloy.

The FT IR spectra of the obtained coatings is presented in Fig. 11 and has presented typical shape characteristic for the Si-DLC layers. For the analysed energy range, the absorption bands have been assigned to the vibrations with the respective bonds indicated below. The bands, located within 2750 ÷ 3000 cm^{-1}, are typical for hydrogenated diamond-like carbon, and have been attributed to the CH stretching vibrations in CH_n (n = 1, 2, 3) and aldehyde groups. The band, centred at around 2085 cm^{-1} and 1401 cm^{-1}, 1346 cm^{-1} corresponds to the vibrations of Si-H and CH_2 bonds, respectively. The band of wavenumbers at 1243 cm^{-1} and peak centred at 766 have been considered as the vibrations of Si-CH_3 bond.

The line at 1000 cm^{-1} may be attributed to the vibrations of Si-0 bonds. However, the line at 762 cm^{-1} has been corresponded to stretching vibrations of $Si\text{-}CH_3$.

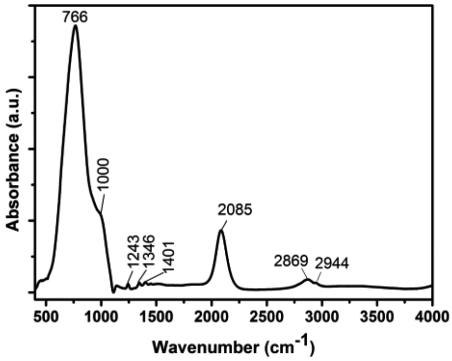

Fig. 11. FT IR spectra of the Si-DLC coatings deposited on Al-Zn alloy using PA CVD method

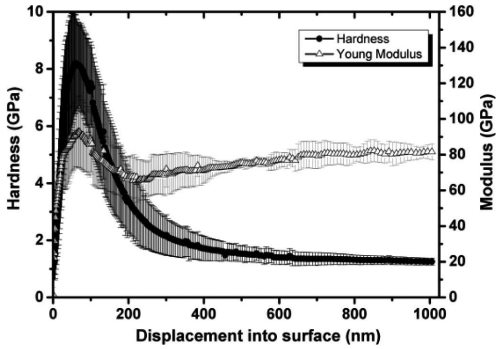

Fig. 12. Hardness and Young modulus profiles of Al-Zn alloy after plasma processes in plasma conditions

The plasma processes applied to aluminium-zinc alloys significantly improved their hardness and Young modulus (Fig. 12) to *ca.* 8.0 GPa and *ca.* 95.0 GPa, respectively.

The increase of nanohardness in the outer coat is probably to due may be explained by the consist of AlN phase in deposition of obtained coatings (XRD analysis) [8]. The microhardness profiles for Al-Zn alloy have confirmed that the modification process *via* N^+ ion and deposition of Si-DLC layers is profitable, since the nanohardness is about four higher in the comparison with reference sample (un-modification Al-Zn alloy).

3.3. Amorphous layers on PEEK

During the last decade PEEK has generated much interest thanks to its thermoplastic properties, chemical resistance, high temperature stability and biocompatibility [9, 10]. It has been considered as a suitable material replacing metals in biomedical implants and as a matrix of carbon fibers composites [11, 12]. But its disadvantage is hydrophobicity and low surface free energy, resulting in poor adhesive properties. In order to improve the properties of PEEK, we modified the samples with ion etching and deposited layers a-CN:H/a-SiCN:H by using RF CVD. The atomic structure and chemical composition of the layers a-CN:H/a-SiCN:H on PEEK were investigated by FTIR and XPS spectroscopic techniques and the layer morphology was studied by SEM/EDS techniques. The SEM image shows the slight effect of surface roughness, but the distribution of nitrogen is uniform on this uneven substrate. It can be found that the obtained layers have a significant degree of homogeneity of chemical composition. The XPS method was used in order to determine the concentration of particular chemical elements in PEEK/a-CN:H/a-SiCN:H samples. The several regions of surface were characterized by XPS depth profiles. It can be noticed that concentration profiles can be divided into three areas of different chemical behaviour (Fig. 13). In the first region (related to the most outer layer directly exposed to the weather conditions) where profiling lasted for 50 minutes, a lot of oxygen of the content approx. of 50 at.%, 29 at.% silica, 18 at.% carbon and 3 at.% nitrogen can be detected. In the second region, where profiling lasted approximately 270 minutes, the concentration of oxygen and silicon in the layer decreases, and the carbon content increases. In the third region, the stabilisation of components of predetermined concentration occurs. The detailed examination of the profiles reveals that at the initial stage of profiling during the first 30 minutes the concentration of all elements hardly changed. In the top region of the layer for the thickness of about 200-250 nm, the ratio of the respective elements corresponding to the stoichiometry $SiC_{0.6}N_{0.2}$ excluding oxygen or to the stoichiometry $SiC_{0.6}N_{0.2}O_{1.7}$ with regard to oxygen. In the first region silicon and carbon dominate and the ratio of N/C = 0.3. After exceeding a depth of 250 nm, the aspect ratio changes, which means that the profiling reached the layer of the type CN:H and the carbon content increases significantly and the amount of nitrogens increases slightly. When the time of profiling reaches 150 minutes at the depth of approximately 500 nm, the ratio of N/C is equal to 0.04/0.33 which gives a stoichiometry $CN_{0.12}H$. Continuing profiling we can see that the quantity of carbon is increasing and content of other elements including oxygen is decreasing.

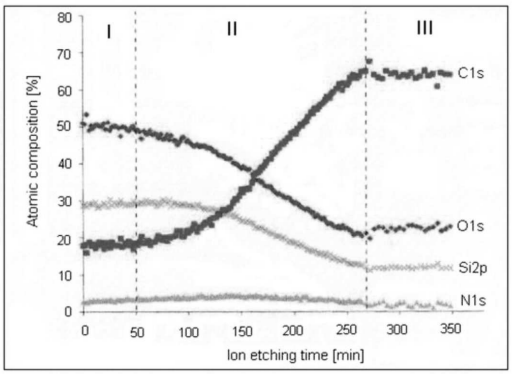

Fig. 13. XPS depth profiles of oxygen, carbon, nitrogen and silica concentrations after ion etching

The FT IR spectra in Fig. 14 for the a-CN:H/a-SiCN:H layers deposited on PEEK show the bands derived from Si-C groups (approx. 800 cm^{-1}) and Si-N (approx. 930 cm^{-1}). There is also visible the intense absorption bands between 1000 cm^{-1} – 1050 cm^{-1} which are related to CH_2 in $SiCH_2$ groups. The contribution to the absorption in this range may also be derived from the stretching vibration of Si-O bond which were formed between the silicon and oxygen adsorbed from the atmosphere due to the high affinity of oxygen to silicon. The spectrum revealed also a narrow band at approx.

1250 cm^{-1} indicating activity of the bending vibration CH_3 in $SiCH_3$ groups. Moreover, the band at 2145 cm^{-1} is shifted to lower frequencies with compared to the spectrum of the layer a-CN:H (ca. 2180 cm^{-1}), which shows the binding C≡N and C≡C.

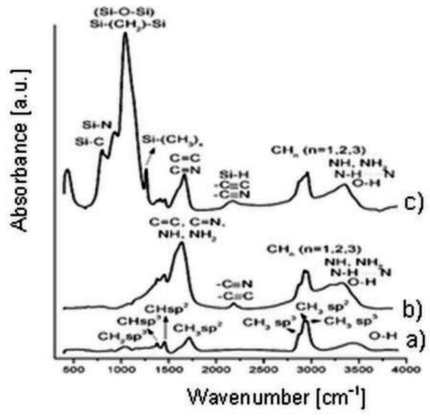

Fig. 14. FTIR spectra measured for (001)Si with layers: a) a-C:H, b) a-CN:H, c) a-SiCN:H

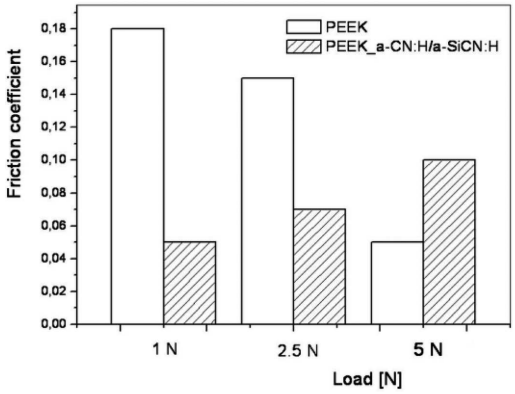

Fig. 15. Friction coefficient measured under various load for unmodified and modified PEEK

The results of tribological studies of the PEEK/a-CN:H/a-SiCN:H presented in Fig. 15 show the variation of the friction coefficient of PEEK with and without the layer changes with the load. The friction coefficient of the PEEK/a-CN:H/a-SiCN:H increase with increasing load. For unmodified PEEK, the reverse dependence is observed. The friction coefficient measured under 1N of least load decreases from 0.18 for unmodified PEEK to 0.05 for the PEEK-layer system. The wear index decreases from $51.4 \cdot 10^{-6}$ mm^3/Nm for unmodified PEEK to $21.7 \cdot 10^{-6}$ mm^3/Nm for the PEEK-layer composite.

The results of contact angles show that unmodified PEEK is rather hydrophobic with water contact angle higher than 80° and moderate value of surface free energy (~44 mJ/m^2), where the polar component is very small (2.5 mJ/m^2). Plasma modification in the Ar atmosphere causes significant decrease of the water contact angle down to 59°, resulting in the significant increase of the total surface free energy up to 56 mJ/m^2, corresponding to huge increase of the polar component of the surface free energy (12 mJ/m^2). PEEK after modification with layers has a hydrophobic character. The value of contact angle increase to 100° and surface energy decrease.

4. Conclusions

Titanium, Al-Zn alloy and PEEK surfaces were successfully modified by PA CVD technique. Ar plasma treatment (plasma etching), nitrogen ion implantation and DLC doped with N and/or Si atoms layers deposition in different combinations (Table 1) were applied with effective improvement of surface parameters.

Our results for the Ti Grade2 (after plasma processes) obtained from the biological and corrosion tests suggest that titanium with the plasmochemically modified surface did not cause severe cytotoxicity against MG63 cells and improve of corrosion properties. In case of Al-Zn alloy (after nitrogen ion modification and SiCH layers deposition) improve of hardness (up to 8 GPa), Young's modulus (up to 6 GPa) and surface smoothness (surface roughness parameter) were observed. Application of plasma modification for polyetheretherketone substrate (CNH and SiCNH deposition layers) resulted in formation of stable surface coatings with a lower coefficient of friction (*ca.* 0.05).

Acknowledgements

This work has been supported by the statutory research of Department of Physical Chemistry and Modeling of Faculty of Materials Science and Ceramics AGH (subject number 11.11.160.257).

REFERENCES

[1] A. Sowińska, T. Borowski, M. Ossowski, M. Kalata, T. Wierzchoń, E. Czarnowska, Inżynieria Materiałowa **3** (187), 2012, 202-205 (2012).
[2] M. Janus, S. Kluska, K. Kyzioł, S. Jonas, S. Zimowski, Inżynieria Materiałowa **3** (187), 177-180 (2012).
[3] S. Fujimoto, N. Ohtake, O. Takai, Surf. and Coat. Techn. **206**, 1011-1015 (2011).
[4] H.R. Allcock, Introduction to Material Chemistry. Wiley&Sons, New Yerk, 2008.
[5] R. Foersch, J Polym Sci: Part A: Polym Chem. **28**, 803-809 (1990).
[6] D. Hegemann, H. Brunner, C. Oehr, Nuc. Instrum. Methods Phys. Res. Sect. B **208**, 281-286 (2003).
[7] F. Awaja, M. Gilbert, G. Kelly, B. Fox, P.J. Pigram, Prog. Polym. Sci. **34**, 948-968 (2009).
[8] K. Kyzioł, S. Kluska, M. Janus, M. Środa, W. Jastrzębski, Ł. Kaczmarek, Surf. Appl. Sci. **311**, 33-39 (2014).
[9] Ch. Oehr, Nucl. Instr. and Meth. In Phys. Res. B **208**, 40-47 (2003).
[10] S.M. Kurtz, J.N. Devine, Biomaterials **28**, 4845-4869 (2007).
[11] D. Briem, S. Strametz, K. Schroeder, N.M. Meenen, W. Lehmann, W. Linhart, A. Ohl, J.M. Rueger, J.Mater. Sci.:Materials in Medicine **16**, 671-677, (2005).
[12] S.M. Kurtz, PEEK Biomaterials Handbook; William Andrew Publishing, Chapter **11**, 163-170 (2011).

Received: 20 February 2014.